photonics

MDPI

Article

Improving the Signal-to-Noise Ratio of Photonic Frequency Conversion from 852 nm to 1560 nm Based on a Long-Wavelength Laser-Pumped PPLN Waveguide Module

Miao Guo [1], Kong Zhang [1,†], Yunhao Zhang [1], Jun He [1,2] and Junmin Wang [1,2,*]

[1] State Key Laboratory of Quantum Optics and Quantum Optics Devices, Institute of Opto-Electronics, Shanxi University, Taiyuan 030006, China
[2] Coaborative Innovation Center of Extreme Optics, Shanxi University, Taiyuan 030006, China
* Correspondence: wwjjmm@sxu.edu.cn
† Current address: Department of Physics and Electronic Engineering, Jinzhong University, Yuci, Jinzhong 030619, China.

Abstract: The storage wavelength of quantum nodes based on atomic systems does not match the wavelength of optical fiber communication, which requires the establishment of an efficient conversion system between flying bits and storage bits. In this paper, based on the nonlinear wavelength conversion technology of the periodically poled lithium niobate waveguide, a low-noise conversion of 852-nm photons to 1560-nm photons was achieved by a 1878-nm pump laser. The generation mechanism and transmission mechanism of noise due to nonlinear process are analyzed theoretically. The noise photons introduced by the spontaneous parameter downconversion and spontaneous Raman scattering process of a strong pump laser are experimentally studied. The noise suppression near 1560 nm is realized by the fiber Bragg grating (FBG) filter. In the experiment, when the FBG bandwidth is reduced from 0.257 nm to 0.130 nm, the signal-to-noise ratio (SNR) increases from 52 to 90. Our results show that the SNR can be greatly improved by using a narrower band filter. Therefore, the quantum node is connected to the fiber channel, and the signal can be transmitted over long distances with low loss and high fidelity.

Keywords: PPLN waveguide; frequency conversion; spontaneous Raman scattering; signal-to-noise ratio

Citation: Guo, M.; Zhang, K.; Zhang, Y.; He, J.; Wang, J. Improving the Signal-to-Noise Ratio of Photonic Frequency Conversion from 852 nm to 1560 nm Based on a Long-Wavelength Laser-Pumped PPLN Waveguide Module. *Photonics* **2022**, *9*, 971. https://doi.org/10.3390/photonics9120971

Received: 7 November 2022
Accepted: 7 December 2022
Published: 11 December 2022

1. Introduction

Quantum frequency conversion (QFC) technology is crucial for constructing the quantum networks that were put forward in 2008. Photon transmission between different quantum nodes is the foundation for realizing quantum repeaters [1,2]. Generally, the physical carriers for quantum memories and quantum processors include single atoms, single molecules, single ions, and single NV color center carriers, as well as spontaneous parametric downconversion, and the four-wave mixing process based on an atomic ensemble. The photons emitted by these quantum nodes are in the visible or near infrared spectral range. Its wavelength is not coincident with the telecom photon, which can transmit in the fiber as low-loss flying qubits to link two different nodes. Therefore, the efficient QFC is required to bridge the gap of the wavelength between the quantum node and telecom band. Based on the above significance, many groups have carried out relevant studies. QFC was first proposed in theory by Kumar in 1990 [3] and was demonstrated in an experiment in 1992 [4]. In 2011, Ikuta's research group [5] realized the downconversion of 780-nm photons to 1522-nm photons with a conversion efficiency of 62%, and proved that the entanglement between the photon and another photon was maintained before and after the conversion. In 2012, Zaske's research group [6] downconverted visible photons emitted by quantum dots at 771 nm to 1313 nm on the communication band, with a conversion efficiency of 30% and signal-to-noise ratio (SNR) of 50. In 2017, Riedmatten's team [7] realized the

information transmission between the cold atoms and another solid-state storage medium through optical fiber. In recent years, the QFC with preserving polarization has been applied to maximize the distance between two entangled nodes in a quantum network. In 2020, Becher's group [8] transformed photons entangled with the atomic spin state from 780 nm to the telecom S band at 1522 nm to realize the generation and observation of entanglement between an Rb atom and a photon at a telecom wavelength transmitted through up to 20 km optical fiber. In the same year, Jian-Wei Pan's team [9] also converted the 795-nm photon to the telecom O band at 1342 nm and realized entanglement over 22 km of field-deployed fiber via two-photon interference, and entanglement over 50 km of coiled fiber via single-photon interference. In 2022, Becher's group [10] further demonstrate heralded entanglement between two independently trapped single Rb atoms generated over 33-km fiber links by converting the 780-nm photons to the 1517-nm photons.

Cesium atomic ensemble is one of the most important quantum memory nodes, which emits photons at 852 nm. The photonic frequency is much higher than that of flying photonic qubits transmitted in the optical fiber networks. In this paper, in order to connect 852-nm Cs D2 transition and 1560-nm telecom C-band, the conversion of 852-nm photons to 1560-nm photons is realized by difference frequency generation (DFG) in a periodically poled lithium niobate (PPLN) waveguide. We analyzed the mechanism of noise introduction theoretically during downconversion. Futhermore, in order to filter out these noise photons and improve the SNR, the influence of different bandwidth filters on SNR are tested experimentally.

2. Theoretical Description of Photonic Frequency Conversion

When light propagates in the medium, due to the electric field component of the light wave, the medium will produce macroscopic electric polarization. If the electric field intensity is strong enough, the high-order term cannot be ignored. Therefore, the second-order nonlinear phenomenon is relatively easy to observe when the dielectric material interacts with light field. The second-order nonlinear polarization is

$$P^{(2)} = \varepsilon_0 \chi^{(2)} E^2. \tag{1}$$

where the ε_0 is the vacuum dielectric constant of dielectric, the $\chi^{(2)}$ is the second order nonlinear polarization rate, and the E is the electric field intensity. Suppose two light fields whose frequency are ω_1 and ω_2 respectively act on the crystal simultaneously:

$$E = E_1 cos(\omega_1 t) + E_2 cos(\omega_2 t). \tag{2}$$

The second-order nonlinear polarization can be expressed as:

$$\begin{aligned} P^{(2)} =& \varepsilon_0 \chi^{(2)} [{E_1}^2 cos^2(\omega_1 t) + {E_2}^2 cos^2(\omega_2 t) + E_1 E_2 cos(\omega_1 t) cos(\omega_2 t)] \\ =& \varepsilon_0 \chi^{(2)} [\frac{1}{2}(E_1^2 + E_2^2) + \frac{1}{2} E_1^2 cos(2\omega_1 t) + \frac{1}{2} E_1^2 cos(2\omega_2 t) \\ &+ E_1 E_2 cos(\omega_1 + \omega_2) t + E_1 E_2 cos(\omega_1 - \omega_2) t]. \end{aligned} \tag{3}$$

It can be seen from the above equation that the output term contains four new frequency generation terms, among which $2\omega_1$ and $2\omega_2$ are second harmonic generation (SHG), $\omega_1 + \omega_2$ is the sum frequency generation (SFG), and $\omega_1 - \omega_2$ is the differential frequency generation (DFG). Theoretically, all four nonzero frequency parts are present; however, usually only one component of the four nonlinear terms appears. Because of that, nonlinear polarization can be efficiently generated only by certain phase matching. In general, this condition does not easily satisfy two nonlinear polarization frequency components synchronously. The waveguide used in this paper can meet the phase-matching condition of DFG. As show in Figure 1, the 1560.5 nm photons are generated by DFG with 852.3-nm photons and 1878-nm photons.

Armstrong et al. first proposed the theoretical assumption of the concept of quasiphase matching in 1962 [11–14]. It is different from the birefringent crystal which needs to be periodically modulated to achieve phase matching when the light waves interact each other. Changing the domain structure of ferroelectric crystals periodically can realize the π phase inversion so that the total phase mismatch of each period is zero between fundamental waves and generated harmonics, thus ensuring efficient generation of harmonics. In our experiment, the PPLN waveguide is used. The cross-sectional area of the waveguide is 20 μm, which can limit the pump light and signal light in a small space, thus increasing the optical power density and improving the conversion efficiency. Theoretically, when the pump laser is strong enough, the maximum conversion efficiency can reach 100%, which is usually not achieved due to the loss of fiber sealing during waveguide fabrication, and some other losses during optical propagation.

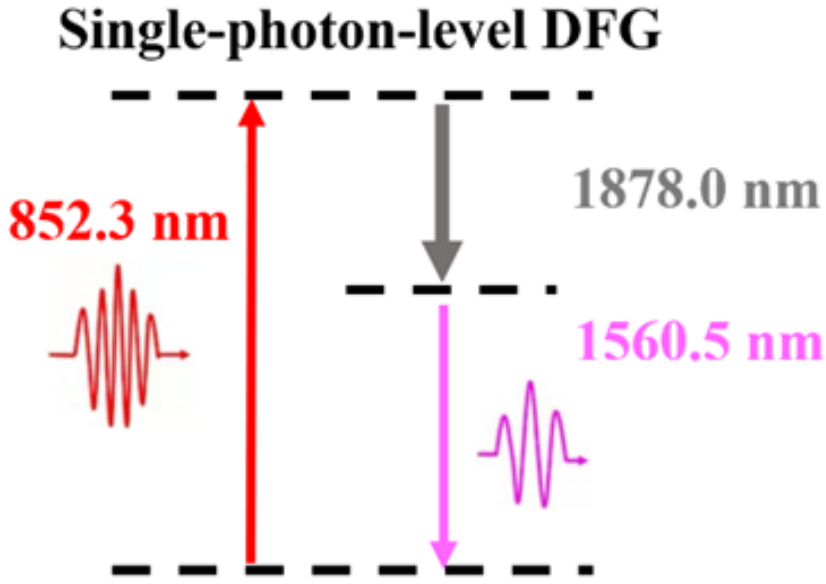

Figure 1. Conversion diagram of the difference frequency generation. The 852.3-nm single photon can be converted to 1560-nm telecom C-band based on 1878-nm long-wavelength pump light.

3. Noise Analysis of Frequency Down Conversion Process

In the process of frequency conversion, both conversion efficiency and SNR are crucial indicators, and many research groups have studied and filtered the noise generated in the process of frequency conversion [15–18]. We analyze the possible noise in the experiment before we design the experimental scheme in detail. When the strong pumping laser is injected into the PPLN waveguide, spontaneous parametric down conversion (SPDC) and spontaneous Raman scattering (SRS) processes also will occur. The SPDC is the combined effect of pumped photon flow and quantum vacuum noise on nonlinear crystals which causes one pump photon to divide into a photon pair, following the laws of conservation of energy and conservation of momentum. The total energy and total momentum of the photon pair is equal to that of pump photon. The SPDC generates noise photons at lower frequency than the pump. In 2010, it was experimentally found by the E.L. Ginzton Laboratory [19] that the SPDC noise photons spectral density from a 1064-nm pump light is 10^6 s^{-1} nm^{-1} when the collection bandwidth is 44 nm. In 2018, Nicolas Maring et al. [20] measured an internal SPDC noise-generation coefficient of 76 kHz/mW/cm normalized to a 1-THz bandwidth. The SRS is a kind of inelastic scattering. The pump laser interacts with the substance so that the substance molecule vibrates, and the photons are scattered at the same time. A strong pump field generally generates Raman noise around its central frequency. The generated photons with a frequency lower than the pump photons are named Stokes photons, and the photons with a frequency greater than the pump photons are named anti-Stokes photons. It has been estimated to have a width smaller than 30 THz.

The anti-Stokes SRS intensity is described by $I(\Delta\nu, T) = I_0\sigma(\Delta\nu)n(\Delta\nu, T)$, where n is the photon occupation number, $\Delta\nu$ is the frequency detuning between the Raman-scattered photon and the pump photon, and T is the temperature [15]. The Raman spectrum for LN is presented in one reference [21] and shows two major peaks at -260 cm^{-1} and -630 cm^{-1}. The authors experimentally find $I_as/I_s \approx 0.11$ by comparing the integrated intensities of anti-Stokes and Stokes Raman peaks. It is confirmed that the intensity of Stokes photons is stronger than that of anti-Stokes photons in experiment. Both of the above spectra are broadband, extending to hundreds of nanometers. In our experiment, we are concerned with the conversion of 852-nm signal photons to the 1560-nm communication band, yet now the nonlinear process of a strong pumping laser in waveguide and fiber during the conversion process may also generate photons near 1560 nm, thus introducing noise. This shows that different pumping laser selection will have different influences on SNR. First, we analyzed the noise based on a short-wavelength pumping laser whose wavelength is 551 nm. As shown in Figure 2, SPDC (green region) and SRS (gray region) processes occur in the waveguide when the strong pumping laser was injected. From the figure, both the noise photons generated from the SPDC and Stokes photons generated from the SRS are located near the signal laser at 852 nm, which will further interact with the pumping laser at 1878 nm and generate noise photons near the target photons at 1560 nm. Due to the limitation of the waveguide's own phase-matching bandwidth, a natural filter is formed. However, it is difficult to distinguish noise photons from target photons. Consequently, it is not conducive to filter the noise generated, and the SNR is relatively low.

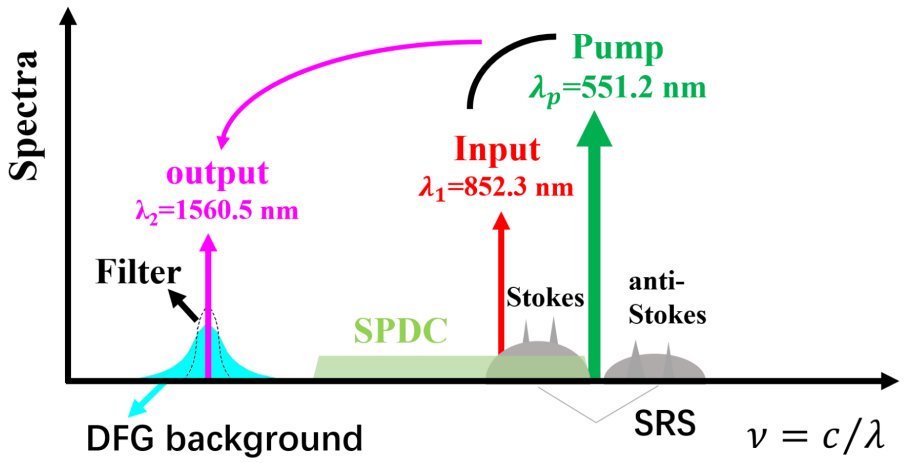

Figure 2. Schematic diagram of the difference frequency generation (DFG) and cascaded DFG. DFG: 852-nm photons near infrared are down converted to 1560-nm photons based on a 551.2-nm pump laser. SPDC, spontaneous parameter down conversion of 551.2-nm pump laser (green area); SRS, spontaneous Raman scattering from 551.2-nm pump laser (Stokes and anti-Stokes photons, gray area); cascaded DFG, differential frequency process between pump laser and noise within the phase-matching bandwidth (blue area).

Then we analyzed the conversion process based on a long-wavelength pumping laser at 1878 nm, as shown in Figure 3. Similarly, SPDC (purple region) and SRS (gray region) processes occur in the waveguide and thulium-doped fiber amplifier (TmDFA), but only the anti-Stokes photons generated by the spontaneous Raman scattering process are located near the target laser at 1560 nm. The anti-Stokes photons are relatively weak and easy to filter, so that the effect of noise can be reduced to a minimum. According to the above analysis, it introduces less noise in the frequency conversion process to select a long-wavelength pumping laser. Therefore, we chose an 1878-nm laser as the pumping laser in the experiment.

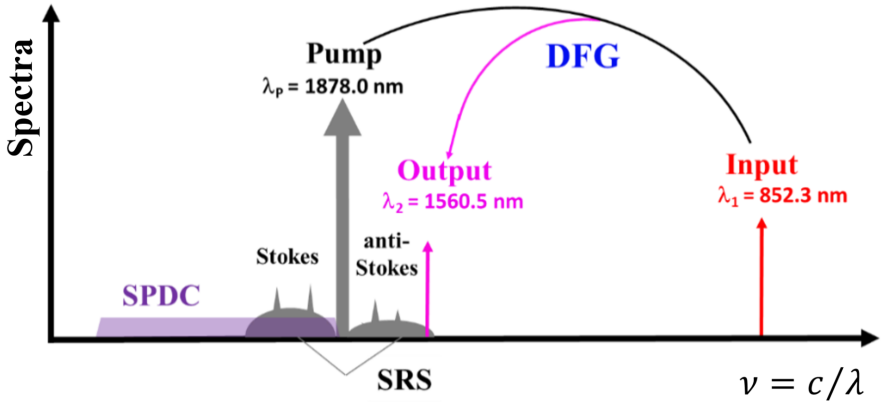

Figure 3. Nonlinear process of conversion of 852-nm photons to 1560-nm photons based on 1878-nm pump laser. SPDC, spontaneous parameter down conversion (purple area); SRS, spontaneous Raman scattering (Stokes and anti-Stokes photons, gray area).

4. Experimental Setup and Experimental Results

4.1. Comparing the Effects of Filters with Different Bandwidths on SNR

Firstly, when 23-mW, 852-nm laser, and a 50-mW, 1878-nm laser were injected, we measured the changing curve of the output power on 1560 nm with temperature and found the best matching temperature. As shown in Figure 4a, we know that the optimized matching temperature of the waveguide is 36.6 °C, and the temperature bandwidth is 6.2 °C through fitting. Then, we test the curve of 1560-nm power with the signal photon wavelength keeping the temperature at 36.6 °C. The phase-matching wavelength is 852.356 nm, and the acceptance bandwidth is 0.548 nm from the Figure 4b.

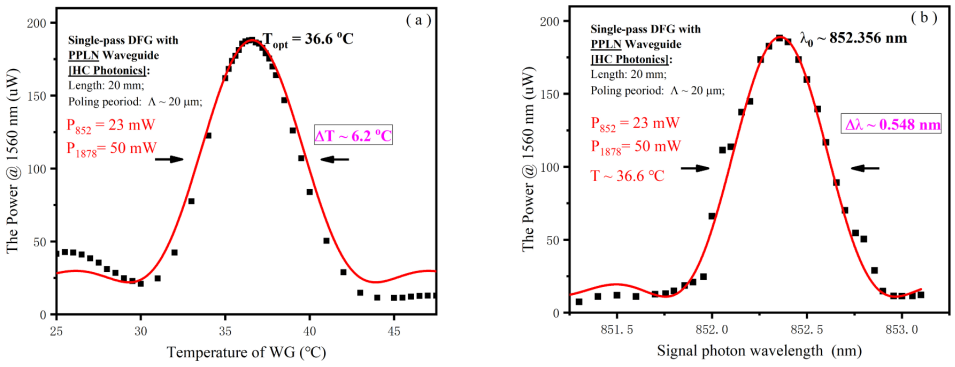

Figure 4. (**a**) Variation curve of DFG conversion power with temperature. (**b**) Variation curve of DFG conversion power with signal photon wavelength. The black squares represent experimental data, and the solid red line represents theoretical fitting curves.

Because the SPDC is a broadband extending to hundreds of nanometers, the noise photons can be filtered with a narrow band filter. Consequently, we further study the effects on noise suppression by using different fiber Bragg grating (FBG) filters with different bandwidths. The experimental setup is shown in Figure 5. The 1878-nm pump laser is provided by a master-oscillator power fiber amplifier (MOPFA) consisting of a seed source and a thulium-doped fiber amplifier (TmDFA). The 852-nm laser is provided by a distributed feedback (DFB) semiconductor laser in a 14-pin butterfly package. Then, the attenuators are used to attenuate the 852-nm laser to 10 pW, which contains 10^9 photons/s. The two laser beams are combined by a wavelength division multiplexing (WDM) into the PPLN waveguide (HC Photonics) with a length of 20 mm. The filter system consists of

1800-nm long-pass filters, a band-pass filter and FBG. Three 1800-nm long-pass filters with 1% reflectivity at 1878 nm and 90% reflectivity at 1560 nm are used to separate the 1560-nm laser from the residual 1878-nm laser when the incidence angle is 45°. The nature of FBG is a grating with periodic phase distribution in the fiber core to form a narrow-band reflection filter. The schematic of the FBG is shown in the inset of Figure 5. It requires a circulator to work with it. The laser output from the waveguide is coupled to the fiber at the first port of the circulator and transmitted to the second port of the circulator. After filtering by the FBG, which is connected at the second port, the laser reflected from FBG is input to the second port and then transmitted to the third port, and finally output. Figure 6 is the reflectance spectrum of three FBGs, with bandwidth of 0.130 nm, 0.195 nm, and 0.257 nm, respectively.

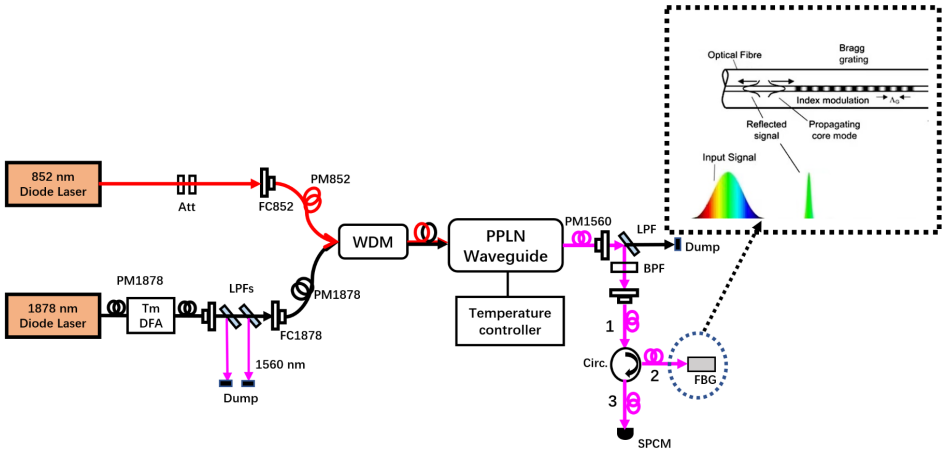

Figure 5. Diagram of experimental device. TmDFA, thulium-doped fiber amplifier; att., attenuator; LPF, long wavelength pass filter; WDM, wavelength division multiplexing; BPF, 1560-nm band-pass filter; Circ., fiber circulator; FBG, fiber Bragg grating filter; SPCM, single-photon counting module.

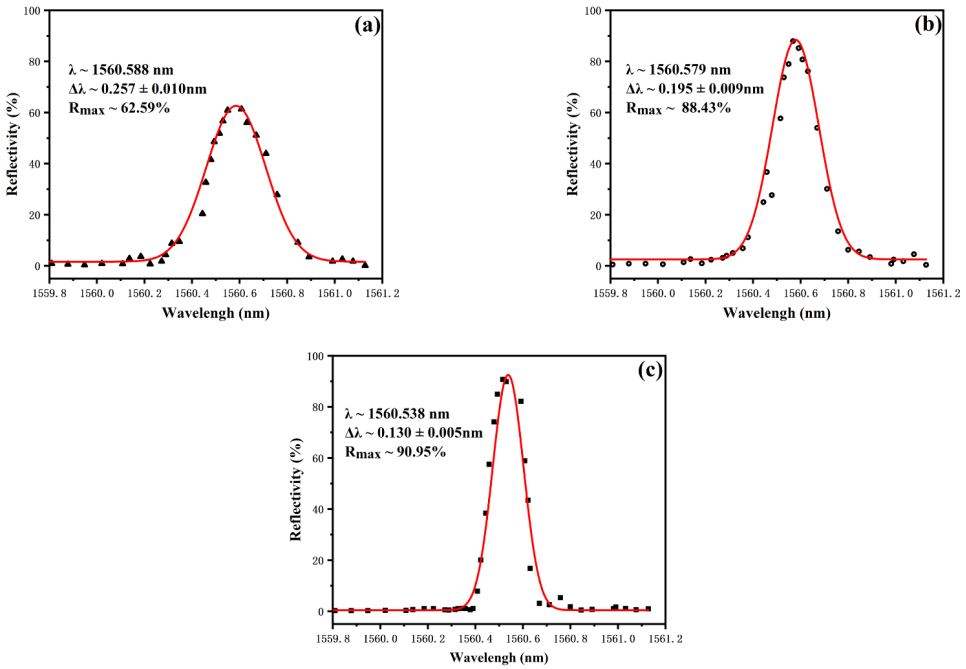

Figure 6. Test results of three FBGs with different bandwidth. (**a**) The result of the FBG with 0.257 nm bandwidth. Its reflectivity is 62.59%. (**b**) The result of the FBG with 0.195 nm bandwidth. Its reflectivity is 88.43%. (**c**) The result of the FBG with 0.130 nm bandwidth. Its reflectivity is 90.95%.

Because that the target photons at 1560 nm cannot completely be separated from the noise photons, the calculation method of Zaske's team is adopted to minimize the impact of noise on the experimental results [21]. The target photons are defined as $N_{out} = N_{p+s} - N_p$, where N_{p+s} represents the counts obtained by injecting the pump laser and signal laser to the waveguide simultaneously, and N_p represents the noise photons counts obtained by injecting only the pump laser. Therefore, the SNR is defined as $SNR = N_{out}/N_p$. Figure 7 shows the effect on noise suppression by using different filters. Figure 7a shows the results of noise counts as an increasing pump power. The blue triangles represent the noise photon count when the bandwidth is 0.257 nm, the red circles represent the noise photon count when the bandwidth is 0.195 nm, and the black squares represent the number of photons when the bandwidth is 0.130 nm. When the pump power is 600 mW, the noise count using 0.130-nm FBG is half of that when using the 0.257-nm FBG. Figure 7b shows the corresponding SNR by using the FBG with different bandwidth, respectively. When the FBG bandwidth is reduced from 0.257 nm to 0.130 nm, the SNR increases from 52 to 90. It can be seen that the SNR has been greatly improved with the narrower bandwidth.

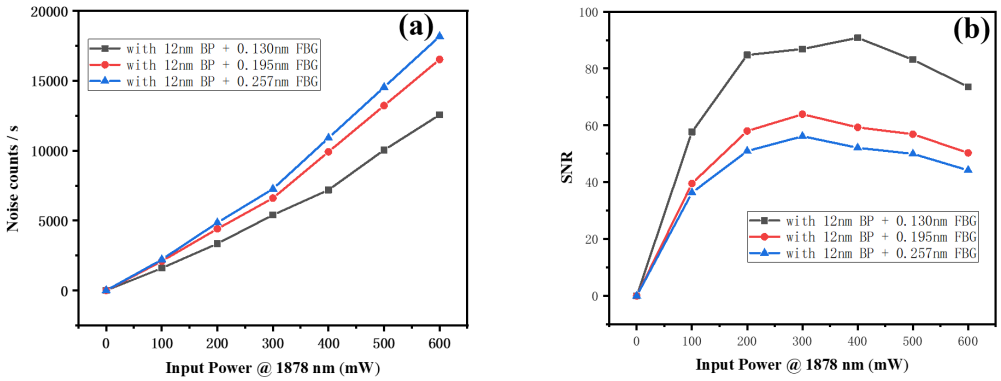

Figure 7. The noise suppression results. (**a**) The noise photon counts results obtained with three filters of different bandwidth respectively. (**b**) The SNR obtained with three filters of different bandwidths, respectively.

In the experiment, the DFG efficiency is defined as

$$\eta = N_{out}/N_{in}, \tag{4}$$

where N_{in} is the number of 852-nm signal photons injected into waveguide, and N_{out} is the number of 1560-nm target photons obtained by conversion. Figure 8 shows the conversion efficiency with increasing pump power. The black square is the result when the bandwidth is 0.257 nm, the red circle is the result when the bandwidth is 0.195 nm, and the blue triangle is the result when the bandwidth is 0.130 nm. The solid line represents the fitting curve of conversion efficiency. The fitting formula is as follows:

$$\eta(P_p) = \eta_{max} sin^2(L\sqrt{\eta_n P_p}), \tag{5}$$

where L is the length of nonlinear crystal, P_p is the pumping laser power injected, and η_n is the nonlinear conversion coefficient [21–23].

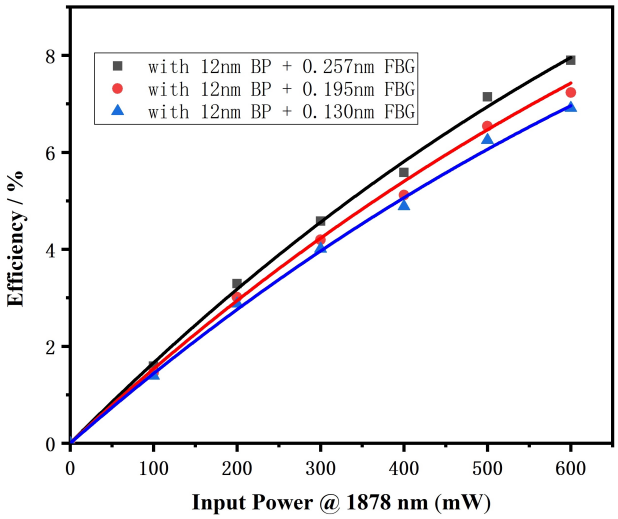

Figure 8. The efficieny with three filters of different bandwidths, respectively.The black squares are the result when the bandwidth is 0.257 nm, the red circles are the result when the bandwidth is 0.195 nm, and the blue triangles are the result when the bandwidth is 0.130 nm.

According to the above experimental data, we made a specific comparison for using the three FBGs with different bandwidths, as shown in Table 1. The first column in the table represents the bandwidth of FBG. The second column represents the maximum SNR, and the corresponding pump power. The third column represents the maximum conversion efficiency, and the corresponding pump power. It can be seen that the narrower bandwidth filter is used, the higher SNR can be attained, whereas the conversion efficiency is not significantly affected.

Table 1. Specific comparison of FBG with different bandwidths in the experimental system.

FBG-Bandwidth	SNR-Max (Pump Power)	η-Max (Pump Power)
0.257 nm	52 (300 mW)	7.9% (650 mW)
0.195 nm	62 (300 mW)	7.2% (650 mW)
0.130 nm	90 (400 mW)	6.9% (650 mW)

4.2. Noise Analysis of Frequency Down Conversion Process

In the above experimental system, the noise photons are also generated from the nonlinear optical process of SRS in the TmDFA near the wavelength of the target photons at 1560.5 nm. In order to filter out the noise photons, we use a series of three free-space long-pass filters placed behind the MOPA laser system at 1878 nm to reflect the photons near 1560 nm and transmit the pump laser at 1878 nm. The noise photons near 1560 nm generated by SRS in the TmDFA can be fully filtered through the above methods. The noise photons with 1800 long-pass filter is compared with that without 1800 long-pass filter when only the 1878-nm pumped laser is injected into the waveguide. The experimental device diagram is shown in Figure 9a, and the experimental results are shown in Figure 9b, where the black squares represent the photons detected when the 1800 long-pass filter is not added, the red circles represent the photons detected when three 1800 long-pass filters are in front of the waveguide, and the blue triangles are the difference between the above two—that are the 1560-nm noise photons generated by the nonlinear process of SRS in the TmDFA. According to the experimental results, after the thulium-doped fiber amplifier, placing the 1800 long-pass filter in front of an optical fiber can reduce the noise photons from 13,000 to 8000 when the power of the pump laser is 700 mW.

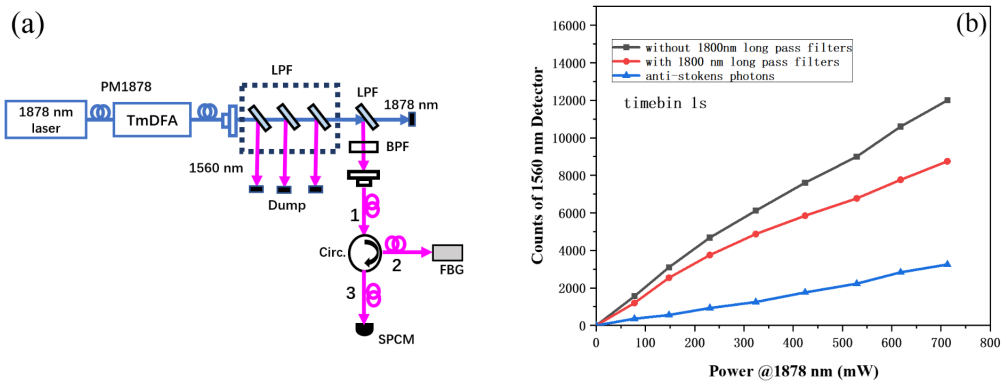

Figure 9. (**a**) The experimental device diagram. (**b**) The data of noise photons from TmDFA with or without 1800 long-pass filter. (T∼1.27%@1560 nm, T∼91.98%@1878 nm).

5. Summary and Outlook

In summary, 852-nm photons, of the Cs atom D2 line, are converted to the 1560-nm photons of telelcom C-band by using a PPLN waveguide, which solves the problem of high loss when 852-nm photons are transmitted via optical fiber. However, due to the fact that the sealing loss of the waveguide we used at present is still relatively large, the conversion efficiency has not become high enough. Subsequently, we will try to optimize the input and output coupling efficiency of the waveguide, or adopt the optimized ridged PPZnO:LN bare waveguide [9]. Reducing the loss caused by fiber sealing and coupling also can further improve the efficiency of DFG. In the process of frequency downconversion, the anti-Stokes photons generated by the spontaneous Raman scattering of the 1878-nm strong pumping laser in the fiber and waveguide are near the target photons at 1560 nm, thus introducing noise. Therefore, in the case of weak laser, we investigate the effects on the conversion efficiency and SNR of the bandwidth of filter. The experimental results show that when the 300-mW pump laser is injected, the SNR is 52 using the FBG with the bandwidths of 0.257 nm, the SNR is 59 when using FBG with bandwidth of 0.195 nm, and the SNR is 90 when using FBG with bandwidth of 0.130 nm. With the bandwidth improving from 0.257 nm to 0.130 nm, the SNR increases from 52 to 90. It can be seen that the narrower the bandwidth of the filter used, the higher the SNR. Hence, we will design a narrow-band temperature-controlled Etalon filter to further filter out the noise near 1560 nm to achieve higher SNR. We subsequently try to use a filter with a higher extinction ratio to further improve the SNR [24]. In addition, we will try to optimize the poling period of the PPLN waveguide to appropriately reduce the quasiphase matching temperature of the waveguide [15], which can also suppress noise photon generation to a certain extent so that the SNR can be improved further. Based on full improvement of the conversion efficiency and SNR, we will proceed, via quantum frequency downconversion, to realize the quantum entanglement between the ultracold Cs single atom captured in the far-detuning optical tweezer and the 1560-nm single photon that is attained from a 852-nm single photon through high efficiency and high SNR frequency downconversion [8–10,25–28].

Author Contributions: Conceptualization, J.W.; methodology, J.W. and J.H.; validation, M.G. and K.Z.; formal analysis, J.W. and J.H.; investigation, M.G., K.Z. and Y.Z.; data curation, M.G.; writing—original draft preparation, M.G.; writing—review and editing, J.W.; visualization, Y.Z.; supervision, J.W. and J.H.; project administration, J.W.; funding acquisition, J.W. All authors have read and agreed to the published version of the manuscript.

Funding: Project supported by the National Natural Science Foundation of China (Grant Nos. 11774210, 11974226, and 61875111).

Data Availability Statement: Data underlying the results presented in this paper are not publicly available at this time, but may be obtained from the authors upon reasonable request.

Conflicts of Interest: The authors declare no conflict of interest.

References

1. Cirac, J.I.; Zoller, P.; Kimble, H.J.; Mabuchi, H. Quantum state transfer and entanglement distribution among distant nodes in a quantum network. *Phys. Rev. Lett.* **1997**, *78*, 3221. [CrossRef]
2. Kimble, H.J. The quantum internet. *Nature* **2008**, *453*, 1023. [CrossRef] [PubMed]
3. Kumar, P. Quantum frequency conversion. *Opt. Lett.* **1990**, *15*, 1476. [CrossRef] [PubMed]
4. Huang, J.; Kumar, P. Observation of quantum frequency conversion. *Phys. Rev. Lett.* **1992**, *68*, 2153. [CrossRef] [PubMed]
5. Ikuta, R.; Kusaka, Y.; Kitano, T.; Kato, H.; Yamamoto, T.; Koashi, M.; Imoto, N. Wide-band quantum interface for visible-to-telecommunication wavelength conversion. *Nat. Commun.* **2011**, *2*, 537. [CrossRef] [PubMed]
6. Zaske, S.; Lenhard, A.; Keßler, C.A.; Kettler, J.; Hepp, C.; Arend, C.; Albrecht, R.; Schulz, W.M.; Jetter, M.; Michler, P.; et al. Visible-to-telecom quantum frequency conversion of light from a single quantum emitter. *Phys. Rev. Lett.* **2012**, *109*, 147404. [CrossRef]
7. Maring, N.; Farrera, P.; Kutluer, K.; Mazzera, M.; Heinze, G.; de Riedmatten, H. Photonic quantum state transfer between a cold atomic gas and a crysta. *Nature* **2017**, *551*, 485. [CrossRef]
8. Leent, T.; Bock, M.; Garthoff, R.; Redeker, K.; Zhang, W.; Bauer, T.; Rosenfeld, W.; Weinfurter, C.B.H. Long-distance distribution of atom-Photon entanglement at telecom wavelength. *Phys. Rev. Lett.* **2020**, *124*, 010510. [CrossRef]
9. Yu, Y.; Ma, F.; Luo, X.Y.; Jing, B.; Sun, P.F.; Fang, R.Z.; Yang, C.W.; Liu, H.; Zheng, M.Y.; Xie, X.P.; et al. Entanglement of two quantum memories via fibres over dozens of kilometres. *J. Abbr.* **2008**, *10*, 142–149. [CrossRef]
10. Leent, T.; Bock, M.; Fertig, F.; Garthoff, R.; Eppelt, S.; Zhou, Y.; Malik, P.; Seubert, M.; Bauer, T.; Rosenfeld, W.; et al. Entangling single atoms over 33 km telecom fibre. *Nature* **2022**, *607*, 69. [CrossRef]
11. Franken, P.A.; Hill, A.E.; Peters, C.W.; Weinreich, G. Generation of optical harmonics, *Phys. Rev. Lett.* **1961**, *7*, 118. [CrossRef]
12. Giordmaine, J.A. Mixing of light beams in crystals. *Phys. Rev. Lett.* **1962**, *8*, 19. [CrossRef]
13. Maker, P.D.; Terhune, R.W.; Nisenoff, M.; Savage, C.M. Effects of dispersion and focusing on the production of optical harmonics. *Phys. Rev. Lett.* **1962**, *21*, 8. [CrossRef]
14. Armstrong, J.A.; Bloembergen, N.; Ducuing, J.; Pershan, P.S. Interactions between light waves in a nonlinear dielectric. *Phys. Rev. Lett.* **1962**, *127*, 1918. [CrossRef]
15. Kuo, P.S.; Pelc, J.S.; Langrock, C.; Fejer, M.M. Using temperature to reduce noise in quantum frequency conversion. *Opt. Lett.* **2018**, *43*, 2034. [CrossRef]
16. Strassmann, P.C.; Martin, A.; Gisin, N.; Afzelius, M. Spectral noise in frequency conversion from the visible to the telecommunication C-band. *Opt. Express* **2019**, *27*, 14298. [CrossRef]
17. Pelc, S.; Ma, L.; Phillips, C.R.; Zhang, Q.; Langrock, C.; Slattery, O.; Tang, X.; Fejer, M.M. Long-wavelength pumped upconversion single-photon detector at 1550 nm: Performance and noise analysis. *Opt. Express* **2012**, *20*, 19075. [CrossRef]
18. Kuo, S.; Pelc, J.S.; Slattery, O.; Kim, Y.S.; Fejer, M.M.; Tang, X. Reducing noise in single-photon-level frequency conversion. *Opt. Lett.* **2013**, *38*, 1310. [CrossRef]
19. Pelc, J.S.; Langrock, C.; Zhang, Q.; Fejer, M.M. Influence of domain disorder on parametric noise in quasi-phase-matched quantum frequency converters. *Opt. Lett.* **2010**, *35*, 2804. [CrossRef]
20. Maring, N.; Lago-Rivera, D.; Lenhard, A.; Heinze, G.; Riedmatten, H.D. Quantum frequency conversion of memory-compatible single photons from 606 nm to the telecom C-band. *Optica* **2018**, *5*, 507. [CrossRef]
21. Zaske, S.; Lenhard, A.; Becker, C. Efficient frequency downconversion at the single photon level from the red spectral range to the telecommunications C-band. *Opt. Express* **2011**, *19*, 12825. [CrossRef] [PubMed]
22. Roussev, R.V.; Langrock, C.; Kurz, J.R.; Fejer, M.M. Periodically poled lithium niobate waveguide sum frequency generator for efficient single-photon detection at communication wavelengths. *Opt. Lett.* **2004**, *29*, 1518. [CrossRef] [PubMed]
23. Langrock, C.; Diamanti, E.; Roussev, R.V.; Yamamoto, Y.; Fejer, M.M.; Takesue, H. Highly efficient single photon detection at communication wavelengths by use of upconversion in reverse-proton-exchanged periodically poled LiNbO3 waveguides. *Opt. Lett.* **2005**, *30*, 1725. [CrossRef] [PubMed]
24. Brunetti, G.; Sasanelli, N.; Armenise, M.; Ciminelli, C. High performance and tunable optical pump-rejection filter for quantum photonic systems. *Opt. Laser Technol.* **2021**, *139*, 106978. [CrossRef]
25. Bock, M.; Eich, P.; Kucera, S.; Kreis, M.; Lenhard, A.; Becher, C.; Eschner, J. High-fidelity entanglement between a trapped ion and a telecom photon via quantum frequency conversion. *Nat. Commun.* **2018**, *9*, 1998. [CrossRef]
26. Law, C.K.; Eberly, J.H. Analysis and Interpretation of High Transverse Entanglement in Optical Parametric Down Conversion. *Phys. Rev. Lett.* **2004**, *92*, 127903. [CrossRef]
27. Ramelow, S.; Fedrizzi, A.; Poppe, A.; Langford, N.K.; Zeilinger, A. Polarization-entanglement-conserving frequency conversion of photons. *Phys. Rev. A* **2012**, *85*, 013845. [CrossRef]
28. Krutyanskiy, V.; Meraner, M.; Schupp, J.; Lanyon, B.P. Polarisation-preserving photon frequency conversion from a trapped-ion-compatible wavelength to the telecom C-band. *Appl. Phys. B* **2017**, *123*, 228. [CrossRef]